Journal of Solid State Chemistry 183 (2010) 373–378

Contents lists available at ScienceDirect

Journal of Solid State Chemistry

journal homepage: www.elsevier.com/locate/jssc

A high temperature superionic phase of $CsSn_2F_5$

P. Berastegui [a], S. Hull [b,*], S.G. Eriksson [c]

[a] Arrhenius Laboratory, Stockholm University, SE-106 91 Stockholm, Sweden
[b] The ISIS Facility, STFC Rutherford Appleton Laboratory, Chilton, Didcot, Oxfordshire OX11 0QX, UK
[c] Department of Chemical and Biological Engineering, Chalmers University of Technology, SE-412 96 Gothenburg, Sweden

ARTICLE INFO

Article history:
Received 3 September 2009
Received in revised form
11 November 2009
Accepted 23 November 2009
Available online 2 December 2009

Keywords:
Superionic conduction
Electron lone-pairs
Neutron diffraction
Impedance spectroscopy
Differential scanning calorimetry

ABSTRACT

The compound $CsSn_2F_5$ has been investigated over the temperature range from ambient to 545 K using differential scanning calorimetry, impedance spectroscopy and neutron powder diffraction methods. A first-order phase transition is observed from DSC measurements at 510(2) K, to a phase possessing a high ionic conductivity ($\sigma \sim 2.5 \times 10^{-2}\,\Omega^{-1}\,cm^{-1}$ at 520 K). The crystal structure of the high temperature superionic phase (labelled α) has been determined to be tetragonal (space group *I*4/*mmm*, a=4.2606(10) Å, c=19.739(5) Å and Z=2) in which the cations form layers perpendicular to the [001] direction, with a stacking sequence CsSnSnCsSnSn… All the anions are located in two partially occupied sites in the gap between the Cs and Sn layers, whilst the space between the Sn cations is empty, due to the orientation of the lone-pair electrons associated with the Sn^{2+}. The structure of α-$CsSn_2F_5$ is discussed in relation to two other layered F^- conducting superionic phases containing Sn^{2+} cations, α-$RbSn_2F_5$ and α-$PbSnF_4$ and, to facilitate this comparison, an improved structural characterisation of the former is also presented. The wider issue of the role of lone-pair cations such as Sn^{2+} in promoting dynamic disorder within an anion substructure is also briefly addressed.

1. Introduction

Superionic conductors are compounds which exhibit exceptionally high values of ionic conductivity (typically $\sigma \sim 0.1-1.0\,\Omega^{-1}\,cm^{-1}$) within the solid state [1,2]. The appearance of 'liquid-like' levels of ionic conductivity at elevated temperatures is associated with extensive dynamic disorder of the conducting ionic species within a rigid substructure formed by the remaining ions. A fundamental understanding of superionic behaviour, and the factors which promote it, has long been a popular research goal, motivated by the desire to elucidate the nature of thermally induced disorder within the solid state. Such issues have also become increasingly important from a more applied point-of-view, to underpin the quest for new materials with high values of ionic conductivity to meet their expanding applications in solid-state battery, gas sensor and fuel cell technologies.

In the specific case of fluoride ion conductors, the majority of compounds displaying superionic conduction at elevated temperatures possess either the fluorite or perovskite crystal structures, or derivatives thereof (for a review, see [2]). However, significant attention has also focused on a small group of ternary compounds within the SnF_2–*M*F (*M*=Na, K, Rb, Cs, Tl, NH_4) phase diagrams, in which the preferred asymmetric anion coordination of the Sn^{2+} cation leads to relatively complex crystal structures characterised by low symmetries and/or larger unit cells. The compounds of stoichiometry $MSnF_3$ are rather poor conductors ($\sigma < \sim 10^{-4}\,\Omega^{-1}\,cm^{-1}$ [3]), despite the presence of large empty channels within the crystal structure which might facilitate anion diffusion [4]. By contrast, several MSn_2F_5 compounds show impressive values of conductivity at temperatures just above ambient, which has been shown to arise predominantly from diffusion of the F^- species rather than electronic conductivity [5,6]. X-ray diffraction studies of KSn_2F_5 [7–10], $RbSn_2F_5$ [11], $TlSn_2F_5$ [12] and $NH_4Sn_2F_5$ [7,13,14] show that all four compounds possess closely related crystal structures. At the highest temperatures, all appear to adopt a rhombohedral structure (α phases) in space group $P\bar{3}$ with Z=1 and $a \sim 4.3$ Å and $c \sim 10$ Å, in which the two cation species form layers perpendicular to the [001] direction with a packing sequence *M*SnSn*M*SnSn… The anions are highly disordered over a number of sites within the gap between the M^+ and Sn^{2+} layers, with highly anisotropic thermal vibrations indicating extensive disorder of the F^- within these two-dimensional planes which is consistent with the high ionic conductivities observed (typically $\sigma \sim 10^{-1}\,\Omega^{-1}\,cm^{-1}$ [3,5,6,12,13,15–20]). On cooling, a number of phase transitions are observed, associated with a lowering of the symmetry, the partial or complete ordering of the anions onto well defined crystallographic sites and a reduction in the ionic conductivity by at least one order of magnitude. Of the

* Corresponding author. Fax: +44 1235 445720.
E-mail address: stephen.hull@stfc.ac.uk (S. Hull).

0022-4596/$ - see front matter © 2009 Elsevier Inc. All rights reserved.
doi:10.1016/j.jssc.2009.11.020

other two MSn_2F_5 compounds, $NaSn_2F_5$ possesses a complex crystal structure [21] and has a low ionic conductivity [3,5], whilst $CsSn_2F_5$ is rather poorly characterised. X-ray diffraction studies of $CsSn_2F_5$ suggested either an orthorhomic [11] or tetragonal [3] unit cell and differential thermal analysis (DTA) studies indicated the presence of a single phase transition at 514 K followed by melting at 570 K [3], though a sequence of three transitions at 440, 510 and 540 K were subsequently reported [6]. The ionic conductivity of $CsSn_2F_5$ was initially reported to be lower than its M=K, Rb, Tl and NH_4 counterparts [5], though other authors found evidence for an increase of around an order of magnitude at $\sim$440 K to a value $\sigma \sim 10^{-2}\,\Omega^{-1}\,cm^{-1}$ [6].

This paper presents a combined differential scanning calorimetry (DSC), impedance spectroscopy and neutron powder diffraction study of $CsSn_2F_5$, with particular emphasis on a superionic phase observed at elevated temperatures in excess of 510(2) K. The resultant information will be compared with two related phases, α-$RbSn_2F_5$ and α-$PbSnF_4$, with an improved structural description of the former also being given.

2. Experimental details

Polycrystalline samples of $CsSn_2F_5$ and $RbSn_2F_5$ of approximate volume 3 cm^3 were prepared from stoichiometric mixtures of the binary fluorides CsF, RbF and SnF_2 supplied by the Alfa Aesar (CsF and RbF) and Sigma Aldrich (SnF_2) chemical companies and of stated purities 99.99%, 99.975% and 99.9%, respectively. After drying, the mixtures were ground to a fine powder in a glove box under an inert atmosphere, pressed into pellets and heated at temperatures of 550 K ($CsSn_2F_5$) and 570 K ($RbSn_2F_5$) for 30 h under a vacuum of 10^{-6} bar. Care must be taken when preparing samples from metal fluoride starting materials, since there is a significant risk that water is present, leading to anion-deficient metal oxyfluorides (see, for example, [22] and references therein). However, such effects would be observed in neutron diffraction experiments as an anomalously high background scattering level (due to the extremely high incoherent neutron scattering cross section of H) or a lower than expected occupancy of the anion sites (since $2 \times F^-$ are replaced by a single O^{2-} and both species have similar scattering neutron scattering lengths). Neither effect was observed in either our starting materials or final compounds.

Thermal characterisation of $CsSn_2F_5$ was carried out using a Perkin-Elmer DSC 2C instrument in the temperature range 300–580 K, with the powder in sealed platinum capsules and at heating and cooling rates of 10 K min^{-1}. Temperature calibration was performed using a standard indium sample. Measurements of the ionic conductivity of the $CsSn_2F_5$ sample used the two-terminal method with impedance spectra collected over the frequency range 10^{-1}–10^7 Hz using a Solartron S1260 Frequency Response Analyser. Pelleted samples of typical dimensions 5 mm diameter and 5 mm length were held between spring loaded platinum contacts and heated at a rate of 0.5 K min^{-1} to a maximum temperature of 545 K.

The neutron diffraction experiments were performed on the Polaris powder diffractometer at the ISIS facility, U.K. [23] with the samples encapsulated inside thin-walled vanadium cans of $\sim$6 mm diameter and $\sim$40 mm height. Diffraction spectra of $CsSn_2F_5$ were collected at 14 temperatures over the range from ambient to 543 K, whilst $RbSn_2F_5$ was measured at a single temperature of 473(3) K. The diffraction studies used the back-scattering detector bank which covers the scattering angles $135^\circ < 2\theta < 160^\circ$ and provides data over the d-spacing range $0.5 < d(\text{Å}) < 3.2$ with an essentially constant resolution of $\Delta d/d \sim 5 \times 10^{-3}$. Indexing and Rietveld refinement of the powder diffraction data used the programs TREOR [24] and GSAS [25], respectively. The quality of the fits was assessed using the usual goodness-of-fit R-factors, R_{wp} and R_{exp} [26].

3. Results

3.1. Differential scanning calorimetry

The DSC curve of $CsSn_2F_5$ shows an endothermic peak indicative of a phase transition at 510(2) K (see Fig. 1(a)), followed by a second peak at 570(2) K corresponding to melting of the sample. These are consistent with one of the previous thermal analysis studies, which reported temperatures of 514 and 570 K, respectively [3], but differ from that reported elsewhere [6]. On cooling, the reverse transitions occurred at the same temperatures, within error. By analogy with the other MSn_2F_5 compounds, we denote the ambient temperature and high temperature phases as β and α, respectively.

3.2. Impedance spectroscopy

Fig. 1(b) shows the ionic conductivity, σ, of $CsSn_2F_5$ as a function of temperature. An abrupt increase in σ of around one order of magnitude is observed at a temperature of 510(3) K, which is in excellent agreement with the temperature of the $\beta \rightarrow \alpha$ phase transition determined by DSC methods (see Section 3.1). At

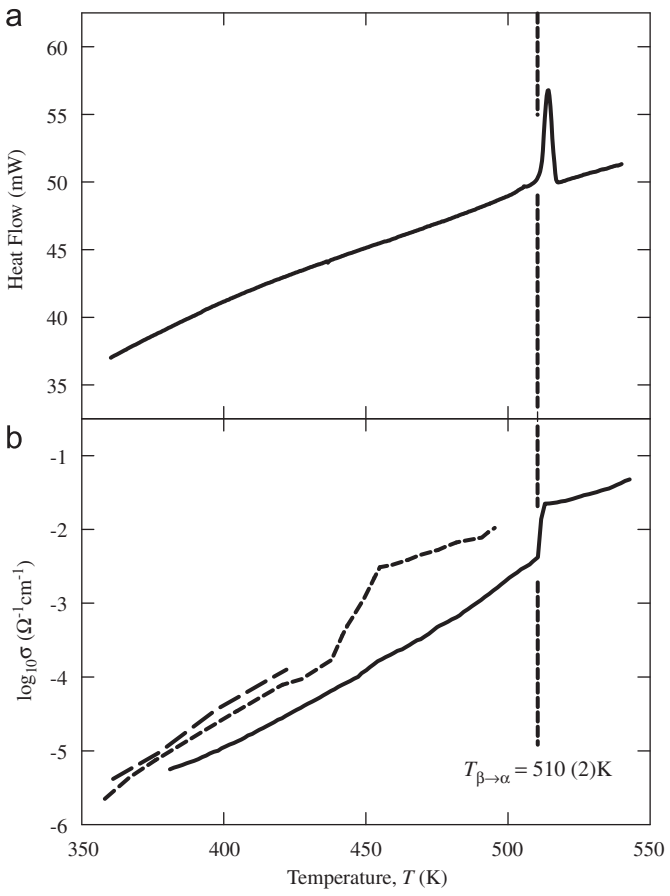

Fig. 1. (a) The DSC curve of $CsSn_2F_5$ showing the thermal event at 510(2) K corresponding to the $\beta \rightarrow \alpha$ phase transition on heating. (b) The temperature variation of the ionic conductivity, $\log_{10}\sigma$, of $CsSn_2F_5$ on heating, showing the abrupt increase at the $\beta \rightarrow \alpha$ phase transition. In the latter case, the solid line denotes this work, whilst the long-dashed and short-dashed lines show the data of Battut et al. [5] and Hirokawa et al. [6], respectively.

relatively low temperatures, the measured ionic conductivity is in fair agreement with the data reported previously by Battut et al. [5] and Hirokawa et al. [6], though the broad increase observed by the latter at temperatures of around 450 K is not reproduced here. The ionic conductivity reaches a value of $\sim 0.04\,\Omega^{-1}\,cm^{-1}$ within the α phase of $CsSn_2F_5$, which is at the lower limit of that generally considered 'superionic' conduction (for comparison, the fluorine ion conductor β-PbF_2 reaches a value of $\sim 1\,\Omega^{-1}\,cm^{-1}$ within its superionic phase [27]).

3.3. Neutron powder diffraction

The presence of a structural $\beta \rightarrow \alpha$ phase transition within $CsSn_2F_5$ on heating is confirmed by the evolution of the neutron powder diffraction pattern with temperature shown in Fig. 2. A significant reduction in the number of Bragg peaks occurs between the measurements performed at 503(2) and 513(2) K. A data collection performed at 538(3) K was used to determine the crystal structure of α-$CsSn_2F_5$. The d-spacings of the observed reflections could be indexed using a tetragonal unit cell of dimensions $a \approx 4.26$ Å and $c \approx 19.7$ Å, which is close to that proposed for the ambient temperature β form on the basis of X-ray diffraction data (a=4.210(1) Å and c=19.103(7) Å [3]). The unit cell volume implies that two formula units are contained within the unit cell, whilst the systematic absences of the Bragg reflections ($h+k+l=2n$ for (hkl); $h+k=2n$ for ($hk0$); $k+l=2n$ for ($0kl$); $l=2n$ for (hhl); $l=2n$ for ($00l$) and $h=2n$ for ($h00$)) imply that the space group symmetry is one of $I4$, $I\bar{4}$, $I4/m$, $I422$, $I4mm$, $I\bar{4}2m$, $I\bar{4}m2$ or $I4/mmm$.

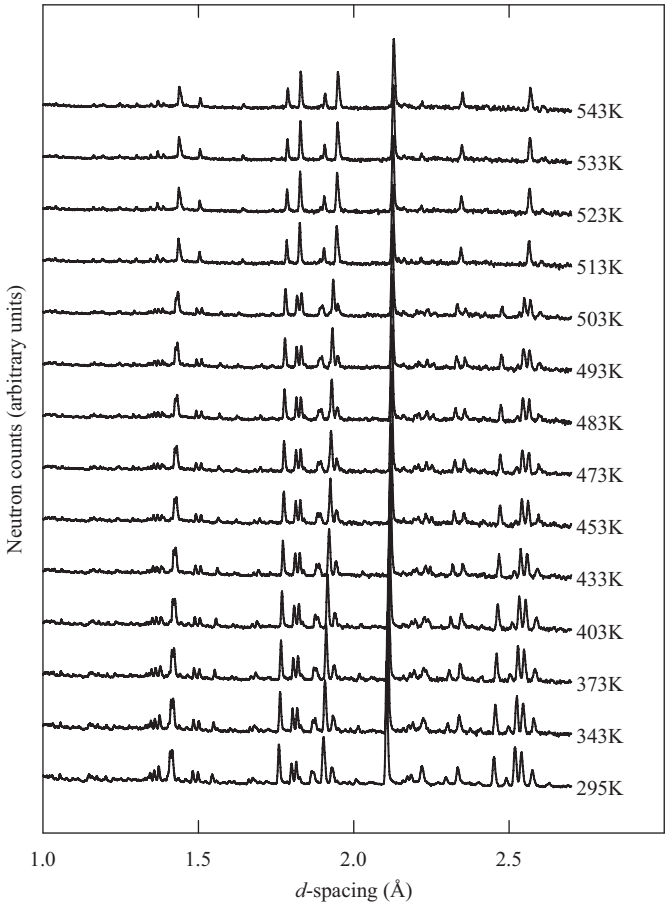

Fig. 2. The evolution of a portion of the neutron diffraction pattern collected from $CsSn_2F_5$ on heating, showing the $\beta \rightarrow \alpha$ phase transition between temperatures of 503(2) and 513(2) K.

The crystal structure of α-$CsSn_2F_5$ was determined by a process of trial-and-error, with the initial models derived from 'chemical sense' and the validity of the final structural model subsequently confirmed by the quality of the fit to the experimental neutron powder diffraction data (see below). It was possible to construct a number of equivalent cation substructures in which the Cs^+ and

Table 1
Summary of the results of the least-squares refinements of the neutron diffraction data collected from α-$CsSn_2F_5$ and α-$RbSn_2F_5$ at temperatures of 538(3) and 473(3) K, respectively.

Phase	α-$CsSn_2F_5$	α-$RbSn_2F_5$
Temperature	T=538(3) K	T=473(3) K
Space group	$I4/mmm$	$P\bar{3}$
Lattice parameters	a=4.2606(10) Å	a=4.3581(6) Å
	c=19.739(5) Å	c=10.1704(14) Å
Unit cell volume	V=358.31(15) Å^3	V=167.29(4) Å^3
Cs/Rb position	2(a) at 0,0,0, etc.	1(a) at 0,0,0.
Anisotropic thermal params	$u_{11}=u_{22}$=0.048(3) Å^2	$u_{11}=u_{22}$=0.0438(8) Å^2
	u_{33}=0.078(4) Å^2	u_{33}=0.0592(15) Å^2
		u_{12}=0.0219(4) Å^2
Sn position	4(e) at 0,0,z, etc., with z_{Sn}=0.33175(17)	2(d) at $\frac{1}{3},\frac{2}{3},z$, etc., with z_{Sn}=0.32839(17)
Anisotropic thermal params	$u_{11}=u_{22}$=0.0518(13) Å^2,	$u_{11}=u_{22}$=0.0727(7) Å^2,
	u_{33}=0.0587(19) Å^2	u_{33}=0.0280(7) Å^2
		u_{12}=0.0363(3) Å^2
$F1$ position	4(e) at 0,0,z, etc., with z_{F1}=0.4310(3)	2(d) at $\frac{1}{3},\frac{2}{3},z$, etc., with z_{F1}=0.13447(17)
Anisotropic thermal params	$u_{11}=u_{22}$=0.201(4) Å^2	$u_{11}=u_{22}$=0.0806(9) Å^2,
	u_{33}=0.068(4) Å^2	u_{33}=0.0428(9) Å^2
		u_{12}=0.0403(5) Å^2
Site occupancy	m_{F1}=1.80(3)	m_{F1}=2 (fixed)
$F2$ position	8(g) at $0,\frac{1}{2},z$, etc., with z_{F2}=0.3565(3)	6(g) at x,y,z, etc., with x_{F2}=0.444(5) y_{F2}=0.199(2) z_{F2}=0.2901(4)
Anisotropic thermal params	u_{11}=0.204(4) Å^2	u_{11}=0.15(3) Å^2,
	u_{22}=0.106(4) Å^2	u_{22}=0.11(3) Å^2
	u_{33}=0.187(6) Å^2	u_{33}=0.077(18) Å^2
		u_{12}=0.041(13) Å^2,
		$u_{13}=-0.012(4)$ Å^2
		$u_{23}=-0.011(4)$ Å^2
Site occupancy	m_{F2}=3.20(3)	m_{F2}=2.17(4)
$F3$ position	–	2(c) at 0,0,z, *etc.*, with z_{F3}=0.2976(7)
Anisotropic thermal params		$u_{11}=u_{22}$=0.148(5) Å^2,
		u_{33}=0.068(7) Å^2
		u_{12}=0.074(2) Å^2
Site occupancy		m_{F3}=0.83(4)
Weighted profile R-factor	R_{wp}=0.76%	R_{wp}=0.59%
Expected R-factor	R_{exp}=0.67%	R_{exp}=0.51%
Number of data points	N_d=3742	N_d=3742
Number of fitted parameters	N_v=36	N_v=44

The anion site occupancies, m, are defined such that the total is that given by the stoichiometry (five). The weighted profile and expected R-factors are given by $R_{wp}^2 = \sum_{N_d} \frac{(y_{obs}-y_{calc})^2}{(\sigma y_{obs})^2} / \sum_{N_d} \frac{(y_{obs})^2}{(\sigma y_{obs})^2}$ and $R_{exp}^2 = (N_d - N_v) / \sum_{i=1}^{N_d} \frac{(y_{obs})^2}{(\sigma y_{obs})^2}$, respectively, and the summations are made over the N_d data points used in the fit. N_v is the number of fitted variables. y_{obs} and y_{calc} are the observed and calculated intensities, respectively, and σy_{obs} is the estimated standard deviation on y_{obs} derived from the counting statistics.

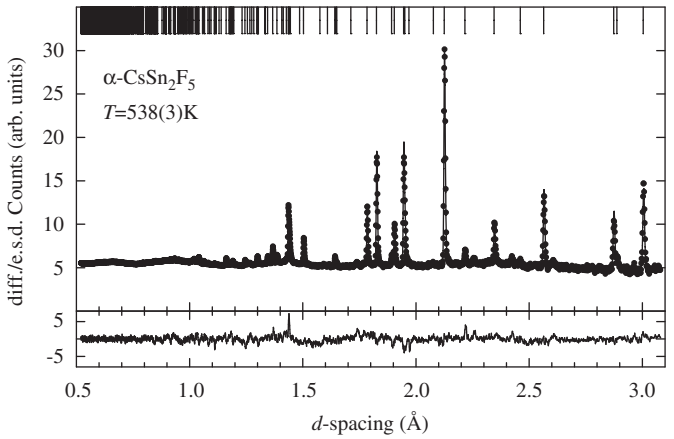

Fig. 3. The least-squares fit to the powder neutron diffraction data collected from α-$CsSn_2F_5$ at 538(3) K. The dots are the experimental data points (with fitted background subtracted) and the solid line is the calculated profile using the parameters listed in Table 1. The lower trace shows the difference (measured minus calculated) divided by the estimated standard deviation on the experimental data points. The row of tick marks along the top of the figure denote the calculated positions of all the symmetry allowed Bragg reflections for space group *I*4/*mmm*.

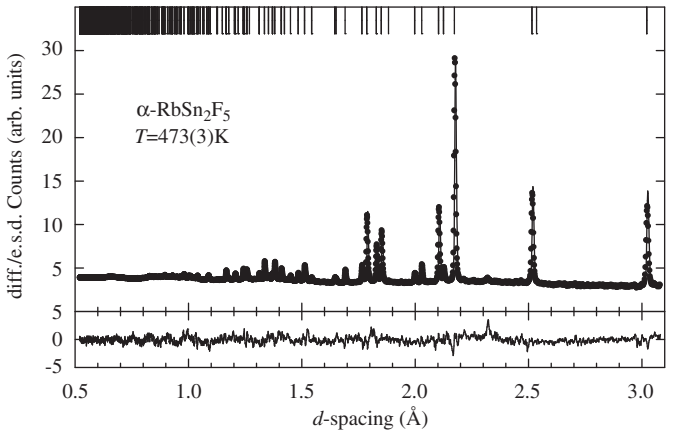

Fig. 4. The least-squares fit to the powder neutron diffraction data collected from α-$RbSn_2F_5$ at 473(3) K. The dots are the experimental data points (with fitted background subtracted) and the solid line is the calculated profile using the parameters listed in Table 1. The lower trace shows the difference (measured minus calculated) divided by the estimated standard deviation on the experimental data points. The row of tick marks along the top of the figure denote the calculated positions of all the symmetry allowed Bragg reflections for space group $P\bar{3}$.

Sn^{2+} are arranged in layers perpendicular to the [001] direction, in a manner similar to that found in the structures of KSn_2F_5 [8–10], $RbSn_2F_5$ [28], $TlSn_2F_5$ [12] and $NH_4Sn_2F_5$ [14]. Of these, the highest symmetry description within space group *I*4/*mmm* places the Cs^+ in the 2(*a*) sites at 0,0,0, etc. and the Sn^{2+} in the 4(*e*) sites at 0,0,*z*, etc., with $z_{Sn} \approx \frac{1}{3}$. A chemically plausible cubic arrangement of anions around the Cs^+ can be generated by placing F^- in the 4(*e*) sites with $z_{F1} = (c\text{-}a)/2c \approx 0.4$. Calculation of the neutron powder diffraction pattern with full occupancy of this anion site (labelled *F*1) gave an encouraging agreement with its measured counterpart and allowed difference Fourier methods to identify that the remaining anions occupy 8(*g*) sites at $0, \frac{1}{2}, z$, etc., with $z_{F2} \approx 0.35$. Rietveld refinement of the experimental data using this structural model gave an excellent fit, with the fitted parameters comprising a scale factor, two lattice parameters, three positional parameters (z_{Sn}, z_{F1} and z_{F2}), two anion site occupancy parameters (m_{F1} and m_{F2}, but subject to the constraint of the chemical stoichiometry, i.e. $m_{F1}+m_{F2}=5$), nine anisotropic thermal vibration parameters, four parameters describing Gaussian and Lorentzian contributions to the instrumental peakshape and 15 coefficients of a shifted Chebyshev polynomial function used to describe the background scattering. The final values of the fitted parameters are listed in Table 1, together with the goodness-of-fit *R*-factors obtained. The quality of the fit to the experimental data is shown in Fig. 3. The partial occupancies and relatively high values of anisotropic thermal vibration parameters for both the anion sites indicate the presence of considerable F^- disorder and are consistent with the high ionic conductivity shown by the α-$CsSn_2F_5$ phase (Fig. 1(b)).

The diffraction pattern collected from the ambient temperature β phase of $CsSn_2F_5$ is rather complex and it has not been possible to solve its structure, despite the apparent relationship between the β and α phases implied by the similarities between their diffraction patterns collected immediately below and above the β→α transition temperature of 510(2) K (see Fig. 2). The structural complexity of β-$CsSn_2F_5$ is probably a consequence of the lower symmetry local coordination preferred by the Sn^{2+} cation and needs to be addressed using single crystal methods.

The α phases of $RbSn_2F_5$ and KSn_2F_5, stable at temperatures above 368 and 428 K, respectively, are reported to be isostructural, with symmetry $P\bar{3}$ and lattice parameters $a \sim 4.2$ Å and $c \sim 10$ Å, such that the unit cell contains only one formula unit [28]. However, to allow a detailed comparison of the structural behaviour of α-$CsSn_2F_5$ and other members of the MSn_2F_5 family of compounds, we have performed a full structural characterisation of the α-$RbSn_2F_5$ phase using neutron powder diffraction data collected at a temperature of 473(3) K. The data were found to be consistent with the structural model for α-KSn_2F_5 reported by Yamada et al. [10]. Within this model, the Rb^+ and Sn^{2+} occupy the 1(*a*) site at 0,0,0 and the 2(*d*) sites at $\frac{1}{3}, \frac{2}{3}, z$, etc., with $z_{Sn} \sim \frac{1}{3}$, respectively; whilst the anions are distributed over three sites labelled *F*1 (2(*d*) sites at $\frac{1}{3}, \frac{2}{3}, z$, etc., with $z_{F1} \sim 0.13$), *F*2 (6(*g*) sites at *x*,*y*,*z*, etc., with $x_{F2} \sim 0.45$, $y_{F2} \sim 0.20$ and $z_{F2} \sim 0.30$) and *F*3 (2(*c*) sites at 0,0,*z*, etc., with $z_{F3} \sim 0.30$), of which the latter two are partially occupied. The final values of the fitted parameters are listed in Table 1, including the anisotropic thermal vibration parameters which are reported here for the first time. The quality of the fit to the experimental data shown in Fig. 4.

4. Discussion

The anion coordination around the Cs^+ within α-$CsSn_2F_5$ is shown in Fig. 5(a). The surrounding eight *F*1 sites are all equidistant from the Cs^+ (at 3.307(2) Å) and form a cubic unit which is significantly flattened along the [001] direction, such that there are eight *F*1–*F*1 distances of 4.261(1) Å and four of 2.726(2) Å. However, since the *F*1 sites are only partially occupied (see Table 1), the mean coordination number of the Cs^+ is only 7.2(1). Each distorted $CsF1_8$ cube shares four of its six faces with neighbouring cubes, forming sheets perpendicular to [001]. The anion environment surrounding the Sn^{2+} is significantly less regular and, as illustrated in Fig. 5(b), comprises a single *F*1 site at 1.959(6) Å plus four *F*2 sites at 2.186(1) Å. Taking into account the partial occupancy of these anion sites, the mean coordination number of the Sn^{2+} is 4.10(5). The geometry of the anion coordination indicates the presence of a stereochemically active lone-pair associated with the Sn^{2+}. To discuss the ionic arrangement within α-$CsSn_2F_5$ further and explore the role of the Sn^{2+} species in promoting superionic conduction we compare its structural properties with those of α-$RbSn_2F_5$ and α-$PbSnF_4$. The latter is a particularly impressive example of the role of lone-pair electrons in promoting extensive anion disorder, and has attracted considerable recent attention because its high ionic

conductivity at ambient temperature ($\sigma \approx 10^{-2}\,\Omega^{-1}\,cm^{-1}$) makes it suitable for use in fast-response gas sensors [29].

The relationship between the structures of α-$CsSn_2F_5$, α-$RbSn_2F_5$, and α-$PbSnF_4$ is illustrated in Fig. 6. In each case the cations are arranged in layers perpendicular to the hexagonal (α-$RbSn_2F_5$) or tetragonal (α-$CsSn_2F_5$ and α-$PbSnF_4$) [001] axes. The individual layers are hexagonal (α-$RbSn_2F_5$) or square planar (α-$CsSn_2F_5$ and α-$PbSnF_4$), with the layer sequence of monovalent M^+ cations and Sn^{2+} ions of *M*Sn Sn *M*Sn Sn… in α-$RbSn_2F_5$ and α-$CsSn_2F_5$ and of PbPbSnSnPbPbSnSn… in α-$PbSnF_4$. The displacement of each layer with respect to its neighbours is approximately $\pm(\frac{a}{3},\frac{a}{3},\frac{c}{3})$ in α-$RbSn_2F_5$, $\pm(\frac{a}{2},\frac{a}{2},\frac{c}{6})$ in α-$CsSn_2F_5$ and $\pm(\frac{a}{2},\frac{a}{2},\frac{c}{4})$ in α-$PbSnF_4$. The anion coordination around the Rb^+ in α-$RbSn_2F_5$ is close to octahedral, which differs from the cubic environment adopted by Cs^+ in α-$CsSn_2F_5$ and presumably reflects the influence of its smaller ionic size [30].

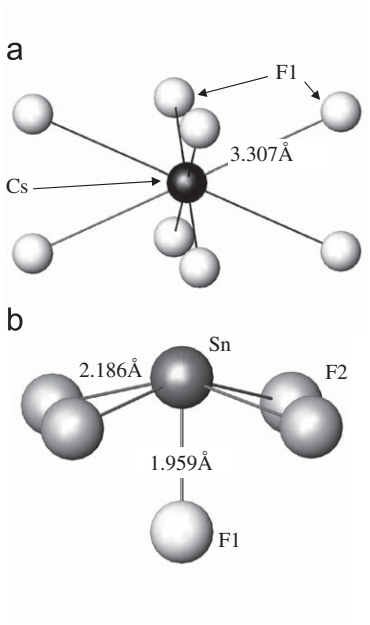

Fig. 5. The fluorine coordination around: (a) the Cs^+ and (b) the Sn^{2+} in α-$CsSn_2F_5$ at 538(3) K.

In all three phases, α-$CsSn_2F_5$, α-$RbSn_2F_5$, and α-$PbSnF_4$, there is no significant anion density within the Sn^{2+}–Sn^{2+} layers and the anion coordination around the Sn^{2+} contains a single F^- along the [001] direction and between three and four F^- forming the highly asymmetric anion environment characteristic of the $5s^2$ lone pair of electrons associated with the Sn^{2+}. However, as illustrated in Fig. 6, the anion distributions are highly distorted and preferentially extend in directions perpendicular to the [001] direction. The high, anisotropic thermal parameters of the anions within the M^+–Sn^{2+} and Pb^{2+}–Sn^{2+} layers and the partial occupancies of many of these sites highlights the presence of extensive F^- disorder and indicates that motion of the anions within these planes gives rise to the high observed ionic conductivities shown by the three phases. For the case of α-$PbSnF_4$, the two-dimensional nature of the anion conduction mechanism has been demonstrated by computer simulations, using ab-initio interionic potentials which treat the presence of lone-pair electrons as an extreme case of electronic polarizibility [31]. These successfully reproduced the time-averaged anion density determined by neutron diffraction studies and showed that anion diffusion is essentially restricted to the Pb^{2+}–Sn^{2+} layers at modest temperatures, with the F^- within the Pb^{2+}–Pb^{2+} layers essentially immobile [31].

5. Conclusions

Numerous factors have been proposed to explain the presence of high temperature superionic behaviour within various anion and cation conducting compounds, including the crystal structure and the properties (size, mass, polarizibility, etc.) of both the mobile and immobile ionic species (for a recent review, see [2]). The presence of 'lone-pair cations' such as Tl^+, Pb^{2+}, Sn^{2+} and Bi^{3+} has been suggested to enhance anion diffusion, because their characteristic asymmetric coordinations can lower the energies of low symmetry interstitial positions that the anions must negotiate as they diffuse between regular lattice sites [32]. Such arguments have, for example, been used to explain the significantly lower superionic transition temperature of the *β*-PbF_2

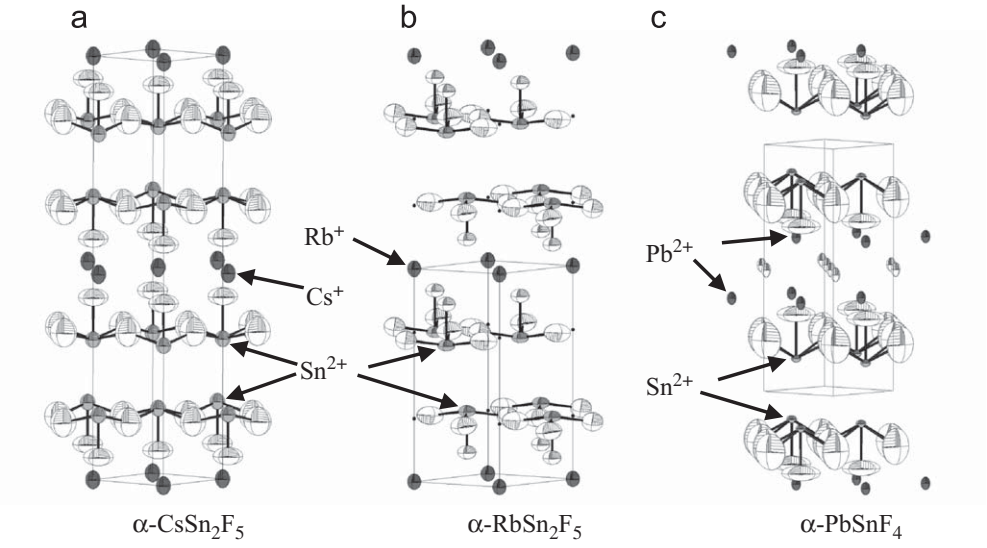

Fig. 6. The crystal structures of (a) α-$RbSn_2F_5$ at 473(3) K, (b) α-$CsSn_2F_5$ at 538(3) K and (*c*) α-$PbSnF_4$ at ambient temperature [31], shown using thermal ellipsoids at the 50% probability level. The dark grey, light grey and white ellipsoids denote the $Rb^+/Cs^+/Pb^{2+}$, Sn^{2+} and F^-, respectively. In the case of α-$RbSn_2F_5$, the F3 sites have a relatively low occupancy (see Table 1) and, for clarity, are shown as small black dots.

compared to other fluorite structured compounds (such as CaF_2 and SrF_2) [33] and to understand the origin of the uniquely high oxide-ion conductivity shown by the high temperature δ phase of Bi_2O_3 [34].

The structural characterisation of the α phase of $CsSn_2F_5$ presented in this paper, together with the descriptions of α-$RbSn_2F_5$ and α-$PbSnF_4$, demonstrate the importance of stereochemically active lone-pairs since, in order to adopt its preferred asymmetric F^- environment, the Sn^{2+} cation generates a highly disordered arrangement of favourable anion positions, with relatively low energy diffusion pathways between them. However, Lacorre has put forward a contrasting view and suggested that a potential route to design new compounds showing high anion conductivities is to start with compounds containing lone-pair cations and replace these species by cations of a similar size but higher valence. In this process, charge compensating additional anions can occupy the sites previously adopted by the electron lone-pair and are able to undergo diffusion through the lattice [35]. This 'lone-pair substitution' mechanism has been demonstrated by the case of $La_2Mo_2O_9$, which has been shown to possess a high oxide-ion conductivity at relatively modest temperatures and has a crystal structure derived from that of the Sn^{2+} containing compound $SnWO_4$ [36]. Clearly, the role of lone-pair cations in promoting extensive dynamic anion disorder is rather complex and depends critically on the specific compounds under investigation.

Acknowledgments

One of the authors (PB) wishes to thank the Swedish Research Council, Vetenskapsrådet, for financial support. The UK Science and Technology Facilities Council is thanked for allocating neutron beamtime at the ISIS Facility. The authors are grateful to Stefan Norberg for his careful reading of the manuscript and suggestions for its improvement.

Appendix A. Supplementary material

Supplementary data associated with this article can be found in the online version at doi:10.1016/j.jssc.2009.11.020.

References

[1] S. Chandra, Superionic Solids: Principles and Applications, North-Holland, Amsterdam, 1981.
[2] S. Hull, Rep. Prog. Phys. 67 (2004) 1233–1314.
[3] S. Vilminot, W. Granier, A. Soufiane, L. Cot, J.-M. Letoffe, P. Claudy, Rev. Chim. Minér. 22 (1985) 125–133.
[4] J.D. Foulon, J. Durand, A. Larbot, L. Cot, A. Soufiane, Eur. J. Solid State Inorg. Chem. 30 (1993) 87–99.
[5] J.P. Battut, J. Dupuis, S. Soudani, W. Granier, S. Vilminot, H. Wahbi, Solid State Ionics 22 (1987) 247–252.
[6] K. Hirokawa, H. Kitahara, Y. Furukawa, D. Nakamura, Ber. Bunsenges. Phys. Chem. 95 (1991) 651–658.
[7] J.D. Donaldson, J.D. O'Donoghue, J. Chem Soc. (1964) 271–275.
[8] S. Vilminot, R. Bachmann, H. Schulz, Solid State Ionics 9–10 (1983) 559–562.
[9] S. Vilminot, H. Schulz, Acta Crystallogr. B 44 (1988) 233–236.
[10] K. Yamada, M.M. Ahmad, H. Ohki, T. Okuda, H. Ehrenberg, H. Fuess, Solid State Ionics 167 (2004) 301–307.
[11] J.D. Donaldson, J.D. O'Donoghue, R. Oteng, J. Chem Soc. (1965) 3876–3879.
[12] S. Vilminot, G. Perez, W. Granier, L. Cot, Rev. Chim. Minér. 17 (1980) 397–403.
[13] N.I. Sorokin, E.G. Rakov, P.P. Federov, R.M. Zakalyukin, Russ. J. Appl. Chem. 76 (2003) 497–499.
[14] A. Soufiane, S. Vilminot, L. Cot, Z. Anorg. Allg. Chem. 556 (1988) 233–239.
[15] M.M. Ahmad, M.A. Hefni, A.H. Moharram, G.M. Shurit, K. Yamada, T. Okuda, J. Phys. Condens. Matter 15 (2003) 5341–5352.
[16] M.M. Ahmad, K. Yamada, T. Okuda, Solid State Commun. 123 (2002) 185–189.
[17] M.M. Ahmad, K. Yamada, T. Okuda, Physica B 339 (2003) 94–100.
[18] W.D. Basler, I.V. Murin, S.V. Chernov, Z. Naturforsh. 36a (1981) 519–520.
[19] W.D. Basler, I.V. Murin, S.V. Chernov, Z. Naturforsh. 38a (1983) 594–595.
[20] I. Murin, A. Peculiunaite, A. Kezionis, R. Mizaras, A. Orliukas, Solid State Ionics 86–88 (1996) 247–250.
[21] R.R. McDonald, A.C. Larson, D.T. Cromer, Acta Crystallogr. (1964)1104–1108.
[22] F.J. Brink, L. Norén, R.L. Withers, J. Solid State Chem. 177 (2004) 2177–2182.
[23] S. Hull, R.I. Smith, W.I.F. David, A.C. Hannon, J. Mayers, R. Cywinski, Physica B 180–181 (1992) 1000–1002.
[24] P.E. Werner, L. Eriksson, M. Westdahl, J. Appl. Crystallogr. (1985)367–370.
[25] A.C. Larson, R.B. von Dreele, Los Alamos National Laboratory Report, LAUR 86-748, 1994.
[26] A.J.C. Wilson (Ed.), International Tables for Crystallography, vol. C, Kluwer, Dordrecht, 1995.
[27] R. Benz, Z. Phys. Chem. 95 (1975) 25–32.
[28] K. Yamada, M.M. Ahmad, Y. Ogiso, T. Okuda, J. Chikami, G. Miehe, H. Ehrenberg, H. Fuess, Eur. Phys. J. B 40 (2004) 167–176.
[29] T. Eguchi, S. Suda, H. Amasaki, J. Kuwano, Y. Saito, Solid State Ionics 121 (1999) 235–243.
[30] R.D. Shannon, Acta Crystallogr. A 32 (1976) 751–767.
[31] M. Castiglione, P.A. Madden, P. Berastegui, S. Hull, J. Phys. Condens. Matter 17 (2005) 845–861.
[32] A. Laarif, F. Theobald, Solid State Ionics 21 (1986) 183–193.
[33] M.J. Castiglione, M. Wilson, P.A. Madden, J. Phys. Condens. Matter 11 (1999) 9009–9024.
[34] C.E. Mohn, S. Stølen, S.T. Norberg, S. Hull, Phys. Rev. Lett. 102 (2009) 155502.
[35] P. Lacorre, Solid State Sci. 2 (2000) 755–758.
[36] P. Lacorre, F. Goutenoire, O. Bohnke, R. Retoux, Y. Laligant, Nature 404 (2000) 856–858.